Chapter 4

DC Microgrid Operation with Hybrid Energy Storage Considering Islanding Constraints and Demand Response Coordination: A Bi-Level Stackelberg Game Approach

4.1 Introduction

DCμGs are becoming popular for rural residential electrification, smart buildings, data centres, PHEV charging stations, etc. [185]. Past investigations suggest that electricity-H_2 sectoral coupling within a μG or IES framework reduces GHG emissions at a competitive price [186, 187], avoids "deep electrification" in industrial, commercial, and transportation sectors [163], provides grid balancing and load regulation services, reduces RES power curtailment, etc. [72, 188]. Moreover, a HESS by coupling BESS with HSS is an attractive option since the complementary characteristics of the two storage mediums can be leveraged to benefit the power system operation [189, 190, 191, 192, 193, 194]. Therefore, research on electricity-H_2 DCμGs has gained traction in recent years [88, 195, 196]. The EMS of an electricity-H_2 DCμG is challenging for several reasons. Firstly, the uncertainties of RES generation, electricity and PHEV charging demand, and wholesale market

electricity price increase the risk of dispatch strategy. The volatility of RES generation can be mitigated by installing an ESS like the BESS for RES generation firming [197] or by consumer-side measures like DR implementation [10]. However, designing a DR implementation framework, coordinating it with the DCμGO scheduling strategy, and balancing the interests of the DCμGO and the flexible consumers considering all operating constraints poses another challenge. The third challenge of designing the DCμG EMS is to incorporate islanding capability so that the DCμG transitions from grid-connected to islanded mode with minimum load curtailment after a fault in the upstream grid without violating network and equipment-level constraints.

This chapter proposes an EMS strategy to tackle the above challenges by co-optimising the electricity and H_2 systems. The aim of the proposed EMS is to incorporate islanding capability in the electricity-H_2 DCμG, balance the interests of the DCμGO (maximise the operating profit) and DR participants (minimise the electricity usage cost of flexible consumers participating in the DR program) considering DCμG network operating constraints, electrical and H_2 system equipment operating constraints, and flexible consumer's apparatus-level constraints. A trade-off between the objectives of the DCμGO and the DR participants is achieved by casting the problem as a bi-level leader-follower Stackelberg game (SG) game.

A literature survey has been presented in **section 1.3**. A comparison of contributions made by relevant papers with the work done in this chapter is given in table 4.1. The following gap areas are found in the existing literature:

- **Gap#1)** To the best of the author's knowledge, an investigation of the interdependence of electrical and H_2 systems together with a HESS has not been reported in the context of DCμG optimal scheduling considering the network operating security constraints (feeder current limits, bus voltage limits) and a DCμG network model. Previous studies, such as [28, 49, 54, 55, 56, 57, 65], [84, 88, 90, 91], and [21, 22, 23, 24, 27, 29, 30, 31, 33, 34, 39, 40, 41, 51, 66, 70, 87, 104, 114], did not focus on leveraging the benefits of HESS and electricity-H_2 sectoral coupling for improving the operating economy and technical performance (like RES generation curtailment) of a DCμG. While some previous studies, such as [12, 78, 79, 80, 81, 86], have focused on leveraging operating and economic benefits of electricity-H_2 sectoral coupling, network model and network operating security constraints of the DCμG

Table 4.1: Summary of Literature review

Ref.	Uncertainties		PHEV	DR	H_2 energy	Objective	Islanding Constraints	DCμG Network constraints
	RVs	Correlation						
[28]	N	N	N	N	N	M	N	N
[65]	B+C	N	N	Y	N	M	N	N
[54]	B	N	Y	Y	N	G+M+O	N	N
[55]	B	N	N	Y	N	G+Q	N	N
[56]	B+C	N	Y	Y	N	R	N	N
[57]	A+B	N	Y	Y	N	G	Y	N
[49]	B	N	N	Y	N	G+Q	N	N
[46]	B	N	N	N	N	G+L	N	N
[63]	A+B+C+D	N	N	Y	N	G+J	N	N
[47]	A+B+C	N	N	Y	N	G	N	N
[58]	A+C	N	Y	Y	N	L	N	N
[75]	N	N	N	N	Y	G	N	N
[79]	A+B+D	N	Y	N	Y	G	N	N
[80]	N	N	Y	N	Y	G	N	N
[81]	N	N	Y	N	Y	G	N	N
[84]	N	N	N	N	Y	G	N	N
[88]	N	N	N	N	Y	G	N	N
[78]	N	N	N	N	Y	G	N	N
[12]	N	N	N	N	Y	G	**	N
[90]	N	N	N	N	Y	P	N	N
[91]	N	N	N	N	Y	P	N	N
[86]	N	N	N	N	Y	G+H	N	N
[21]	N	N	Y	Y	N	G+I	N	N
[51]	N	N	N	N	N	G	N	N
[104]	N	N	N	Y	N	H+L	Y*	Y
[114]	N	N	N	N	N	G	N	N
[24]	N	N	N	Y	N	G	N	N
[22]	N	N	N	N	N	G	N	N
[23]	N	N	N	N	N	G+L	N	Y
[29]	N	N	N	N	N	G	N	Y
[27]	N	N	N	N	N	H	N	Y
[30]	N	N	N	Y	N	I	N	N
[31]	N	N	N	N	N	H	N	Y
[34]	N	N	Y	N	N	G	N	Y
[70]	B+C	Y	N	N	N	L	N	N
[87]	N	N	N	N	Y	G	N	N
[39]	N	N	N	N	N	I	N	N
[66]	B+C	N	N	N	N	G+J+K	N	Y
[40]	N	N	N	Y	N	G+H+I	N	N
[33]	N	N	N	N	N	L	N	N
[41]	N	N	N	N	Y	G+H+L	N	Y
CW	A+B+C+D+E+F	Y	Y	Y	Y	G	Y	Y

A: Wind B: Solar C: Load D: Price E: PHEV F: Temperature G: Min cost H: Min loss I: Max load expectation ratio J: Min emission K: Small-signal stability improvement L: Voltage profile improvement M: Max user satisfaction O: Self-sufficiency P: Fuel consumption minimisation Q: Min prosumer discomfort R: Max profit N: No Y: Yes CW: Current work **: Resilience-oriented scheduling with predefined islanding period Y*: Predefined scheduled islanding.

system were not incorporated in the above studies. Since the network model and network operating constraints of the DCμG system were not incorporated in the EMS proposed in [12, 78, 79, 80, 81, 86], the optimal solutions of the EMS may lead to network operating constraint violations (over/under voltage and feeder overloading). A comprehensive study on the EMS of a coupled electricity-H_2 DCμG with an HESS considering the network model and network operating constraints is required to circumvent the above issue.

- **Gap#2)** To the author's knowledge, most researchers have not considered islanding constraints with uncertain islanding instant in the scheduling model of a DCμG. Under normal operating conditions, a DCμG operates in grid-connected mode. The DCμG switches to island operation when there is a disturbance in the upstream grid [185]. The unintended islanding instant is uncertain and not known as apriori. In other words, the islanding can occur at any time within the scheduling horizon. The line flows, bus voltages, generator, and storage system outputs in island mode will deviate from the pre-islanding values. However, no network and equipment constraints should be violated after unintended islanding for a secure and reliable operation. Moreover, the existing storage units and available generation within the DCμG should continue to supply the DCμG load with minimum load curtailment after islanding. The same can be guaranteed by formulating and incorporating islanding constraints in the EMS of a grid-connected DCμG. However, to the author's knowledge, this aspect has not received sufficient attention so far.

- **Gap#3)** Coordination of DR participation with DCμGO resource scheduling to balance the interests of the DCμGO and flexible consumers considering flexible consumer's apparatus level model and constraints have not received sufficient attention. Many papers dealing with DR implementation in a DCμG system have considered an aggregated model of flexible loads [12, 78, 104, 198]. However, an aggregated model of flexible loads cannot accurately account for consumer preferences and requirements like thermal comfort (e.g., the indoor temperature of a room cooled by a TCL/air con), time-dependent energy requirement of a PHEV participating in the DR program, DOC and DOD constraints of PHEV batteries, etc. Hence, apparatus-level models of flexible loads participating in the DR program should be

considered for more accurate and practical representation.

- **Gap#4)** The correlations between input uncertain RVs have rarely been considered in the studies dealing with the EMS of a DCμG. The authors in [70] used Inverse Nataf transformation to model the correlation between SPG power and load demand in the EMS of an islanded DCμG. However, correlations between other input RVs (like WPG and SPG power, load and WPG power, ambient temperature and WPG power, ambient temperature and SPG power, ambient temperature and load demand) were not considered. Therefore, a more detailed investigation of correlations between all relevant correlated input RVs is needed for a more practical and detailed study.

In a nutshell, to the best of the author's knowledge, no comprehensive study on co-optimisation of H_2 and electricity systems within a DCμG architecture has been reported so far, which simultaneously deals with leveraging the flexibility of a HESS and coordinated DR participation considering apparatus-level models (instead of an aggregated model of flexible load), incorporation of islanding capability, consideration of DCμG network and equipment level constraints, and correlated uncertainties of input RVs (see table 4.1). This chapter addresses the above research gap.

In this chapter, a bi-level probabilistic SG-based EMS is proposed for a grid-connected electricity-H_2 DCμG with a HESS incorporating islanding constraints and with coordination between the operation of the DCμG and DR participators. The uncertain input RVs are modelled in the probabilistic domain using a copula-embedded Monte Carlo dynamic averaging approach and incorporated in the EMS module. The objective of the DCμGO is to maximise the day-ahead profit for grid-connected operations using available generation sources and grid power, HESS (BESS and HSS), and controllable loads subject to equipment and network operating constraints. On the other hand, the objective of flexible consumers is to minimise the cost of day-ahead electricity usage. The DR participation is coordinated with the DCμG operation using a bi-level SG game. Investigations in [12, 78] have incorporated resilience in the scheduling scheme of coupled electricity-H_2 systems. However, the above studies considered that the islanding occurs within a pre-defined operating period, and network-level constraints were not incorporated in the scheduling scheme [12, 78]. Also, the study in [104] considered pre-defined islanding in-

stant. In contrast, the contribution of the proposed EMS is to consider uncertain DCμG islanding (from an islanding time viewpoint) in the bi-level optimal scheduling problem, i.e., the islanding can occur at any time within the scheduling period. Therefore, the proposed model allows the DCμG to operate in island mode and supply the loads within the DCμG when the time of the main grid disturbance is unknown, subject to equipment and network operating constraints. Therefore, contributions of the EMS proposed in this chapter are as follows:

- **Contribution#1)** *To address the first gap, an EMS is designed for an electricity-H_2 grid-connected DCμG with a HESS incorporating DCμG network and equipment level constraints*: The flexibilities of P2H unit, H2Punit, and HESS are explored in the context of DCμG operation not only to improve the economic viability in the grid-connected mode but also to guarantee secure operation with minimum load curtailment during island operation. Further, DCμG network-level and equipment-level operating security constraints are modelled and included in the energy scheduling scheme.

- **Contribution#2)** *To address the second gap, constraints of islanding capability are formulated and included in the EMS considering DCμG network and equipment level constraints*: A probabilistic EMS of the grid-connected electricity-H_2 DCμG with a HESS is developed considering constraints of islanding capability. In the present work, the time instant of islanding is uncertain. Incorporating islanding constraints in the EMS yields optimal setpoints of controllable resources within the DCμG for grid-connected operation while simultaneously ensuring sufficient reserve capacities for satisfactory operation with demand-generation balance in a post-islanding scenario without violation of the operating constraints of the network and equipment. More specifically, incorporation of the islanding constraints in the DCμG EMS will ensure the following after unintended islanding: a) Load-generation balance is maintained; b) Dispatchable generators, P2H, and H2P units are not overloaded; c) DOC and DOD of BESS and HSS are not violated; d) Feeders are not overloaded, e) and bus voltages remain within limits.

- **Contribution#3)** *To address the third gap, a bi-level EMS model is proposed for coordinating DCμGO scheduling with DR participation considering apparatus level*

models/constraints of flexible loads and a dynamic RPP scheme: DR participation of flexible consumers is coordinated with the operation of the DCμG by modelling the EMS as a leader-follower SG. The DCμGO is the leader, and the DCμG consumers are followers. The aim of the DCμGO is to maximise the profit during grid-connected operation, while that of the flexible consumers is to minimise the electricity usage cost. The DCμGO optimally schedules resources within its control considering the islanding constraints and sets the RPP. The consumption pattern of flexible loads (PHEVs and TCLs, i.e., air con) is optimised according to the set RPP to minimise energy usage costs. Unlike the aggregated flexible load model used in many previous works on DCμG scheduling [12, 78, 104, 198], apparatus-level models are used to represent flexible loads in this work, making the proposed model more practical.

- **Contribution#4)** *To address the fourth gap, correlations between all correlated input RVs like SPG and WPG power, non-flexible load demand, and ambient temperature are modelled using the Copula-based approach*: Input RV uncertainties and their correlation are modelled using "Frank Copula" and incorporated into the DCμG EMS for minimising the risk of dispatch strategy.

The rest of this chapter has the following structure. The proposed model is developed in **section 4.2**. Numerical studies and conclusions are given in **section 4.3** and **section 4.4**, respectively.

4.2 Materials and methods

4.2.1 DCμG structure and operation

The DCμG operates in grid-connected mode during normal operation but switches to island mode during a fault in the upstream grid. The DCμG is connected to the upstream grid through a GIC, which allows the DCμG to draw power from the upstream grid during grid-connected operation. The operation of the DCμG is managed by a DCμGO. The DCμGO owns RES units (WPG and SPG), GT, P2H, H2P, BESS, and HSS. The DCμG not only supplies electrical consumers but also caters to some H_2 consumers. The H_2 consumers are not necessarily physically located within the DCμG and can be an

industry that consumes electricity from the upstream AC distribution system but has a H_2 purchase contract with the DCμG.

The optimal scheduling strategy of the DCμGO depends on the load demand of the electricity consumers. The electricity consumers comprise non-flexible and flexible loads. Flexible loads (PHEV and TCL/air con) participate as DR entities. The optimal scheduling problem of the DCμGO is coordinated with the power consumption scheduling of flexible consumers using a bi-level SG optimisation framework, in which the DCμGO is the leader and the consumers are followers. The upper and lower-level objectives are designed to maximise the profit of the DCμGO and minimise consumers' energy usage costs. A dynamic RPP mechanism bridges the upper and lower levels. The power trading between the DCμGO and the consumers occurs at RPP. The framework of the leader-follower SG is as follows:

$$\mathcal{J} = \{\{\text{DC}\mu\text{GO, consumers}\}; \{\pi_t^{R,b}\}; \{PFL_t^b\}; \{\mathcal{W}_1, \mathcal{W}_2\}\} \tag{4.1}$$

where {DCμGO, consumers}: set of participants in the game, $\{\pi_t^{R,b}\}$ and $\{PFL_t^b\}$: strategies of DCμGO and consumers at time t, $\{\mathcal{W}_1, \mathcal{W}_2\}$: sets of objectives in the game. The DG units and the flexible consumers are small. Therefore, they cannot participate in the energy market transactions independently. The DCμGO is an intermediary between the electricity market and individual units and participates as a price-taker (due to limited capacity) in the day-ahead energy-market transactions by aggregating available DG (RES, FC, and GT) units, BESS, HSS, P2H, and flexible consumers. The DCμGO (leader) aims to collaboratively optimise the internal flexible resources based on the day-ahead energy-market price and the flexible and non-flexible load demands of the consumers for maximising its profit while meeting all technical constraints of the DCμG equipment, network, and consumer electricity demand. The DCμGO guides the energy consumption pattern of the flexible consumers by setting the RPP. The strategy of the DCμGO,i.e., RPP ($\pi_{t,b}^R$), is communicated to the followers (consumers). Flexible consumers schedule energy consumption according to the propagated RPP to minimise the cost of energy consumption. The flexible power demand profile (PFL_t^b) is the strategy of the consumers, which is fed back to the leader (DCμGO). The leader (DCμGO) re-optimises the scheduling of DER and offers its updated strategy, i.e., the RPP ($\pi_t^{R,b}$), to the consumers. The consumers again rework their strategies (PFL_t^b) based on the updated RPP and propa-

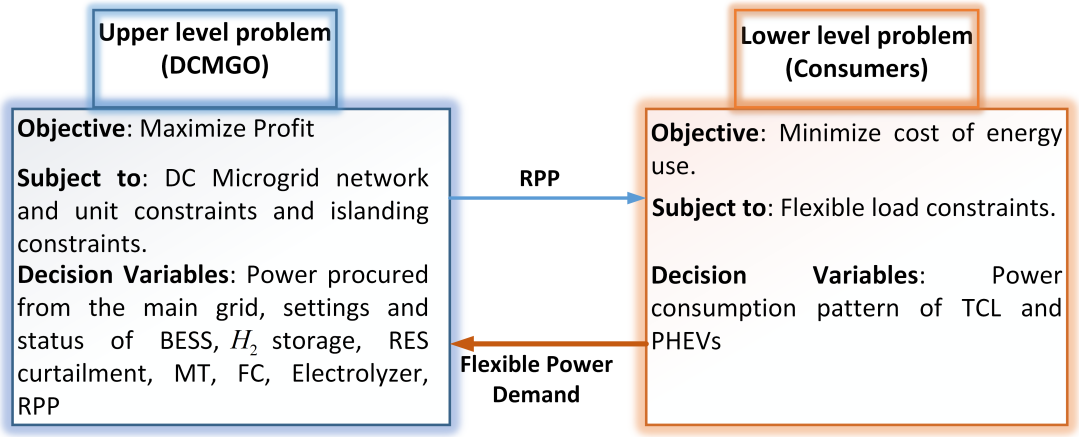

Figure 4.1: Structure of the bi-level SG game

gate the information to the leader (DCμGO). The iteration process continues till every player obtains satisfactory results, i.e., the SG equilibrium is achieved, and players do not deviate from the equilibrium. The operation model is shown in fig. 4.1.

If the load demand is high when the energy price in the upstream wholesale energy market is high, the DCμGO is forced to procure energy from the wholesale market at a high price and operate relatively non-economical units to cater to the load demand. Therefore, the operating cost of the DCμGO increases, and the profit of the DCμGO reduces. On the other hand, if the power consumption of the flexible loads is reduced during periods of high energy price in the wholesale market and moved to periods where the energy price in the wholesale market is low, then the operating cost of the DCμGO and the stress on the DCμG network will reduce. This is achieved by guiding the consumption pattern of flexible loads participating in the DR program. Through the dynamic RPP mechanism of the bi-level SG, the DCμGO sets a high RPP when the energy price in the wholesale energy market is high and a low RPP when the wholesale market energy price is low. In response, flexible consumers modify their energy demand profile to reduce energy consumption during periods of high RPP and increase energy consumption during periods of low RPP, thereby minimising the cost of their energy usage. Therefore, flexible consumers have sufficient motivation to adjust the electricity demand and participate in the DR program. The operating cost of the DCμGO also reduces since the flexible load demand is reduced when the energy price is high in the wholesale market.

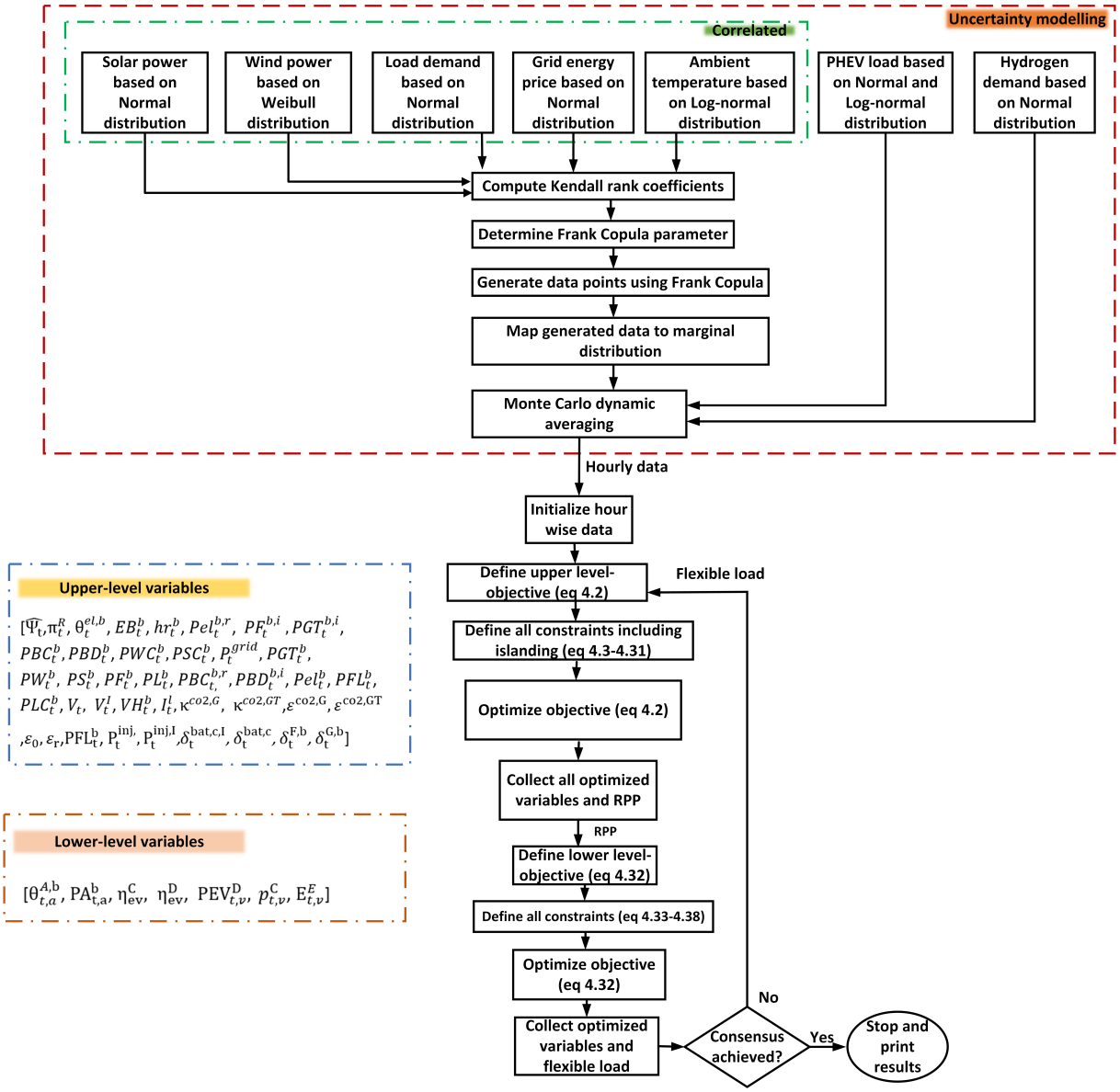

Figure 4.2: Flowchart of the proposed approach in a bi-level optimisation framework

4.2.2 Modelling of uncertainties

The hourly uncertainties of input RVs are modelled by pdf in the probabilistic domain. Uncertain input RVs are WPG and SPG generation, load demand, upstream electricity price in the wholesale market, ambient temperature, H_2 demand, Driven distance (DD) and Subsequent trip distance (STD) of PHEVs, arrival and departure time of PHEVs. The H_2 demand, DD, STD, arrival and departure times are considered to be uncorrelated RVs. The H_2 demand is modelled by "normal" distribution, while the DD and STD are modelled by "log-normal" distributions [173]. On the other hand, arrival and departure times follow "normal" distributions [173].

Input RVs like RES (i.e., WPG and SPG) generation, electricity demand, electricity price in the day-ahead energy market, and ambient temperature are interdependent [199, 200]. Correlation between input RVs significantly impacts the aggregated uncertainty in the overall system [199, 200]. "Copula" is used to model correlated input RVs. A joint multivariate normal distribution can be used if the correlated RVs follow normal marginal distributions [199]. However, if the correlated input RVs do not follow normal distributions, the dependency structure can be modelled using "copula" theory [199, 200]. Based on Scalar's theorem, copula allows the expression of multivariate distribution in terms of univariate marginal distribution and a copula function [201]. Therefore, copula has been used in this chapter to model the dependency structure of correlated input RVs.

Hourly data of correlated input RVs of Sardinia, Italy are adopted from "ENTSO-E Transparency" and "PVGIS" platforms [179, 180] and best-fit univariate distributions are ascertained for each of the correlated input RVs. "Normal" distribution best fits load demand, electricity price in the wholesale market and SPG power, while "Weibull" and "Lognormal" distributions fit into the dataset of WPG power and ambient temperature, respectively. Hourly "Kendall" rank coefficients are found for each pair of correlated input RVs [202]. Some correlated input RVs show negative correlations. "Frank Copula", belonging to the family of "Archimedean Copula", can model both positive and negative correlations [203]. Therefore, "Frank Copula" is used to model correlated input RVs. Hourly values of "Frank Copula" parameters are determined from the "Kendall" rank coefficients and used to generate $20,000$ data pairs for each correlated input RVs at each hour. The randomly generated data are mapped back to the inverse univariate distribution [202]. "Monte Carlo dynamic averaging" method is employed to find the most likelihood values of both correlated and uncorrelated input RVs [181], which are then fed to the EMS. The flowchart of the bi-level problem is shown fig. 4.2.

4.2.3 System model

4.2.3.1 Upper-level problem

The objective of the DCμGO is to maximise the profit, and is given as follows:

$\max(\hat{\mathcal{W}}_1), i.e., \min(\mathcal{W}_1), \mathcal{W}_1 = -\hat{\mathcal{W}}_1;$

$$\hat{\mathcal{W}}_1 = \sum_{t\in\mathcal{T}}(\sum_{b\in\mathcal{B},b\neq 1} (\pi_t^{R,b}(PFL_t^b + PNFL_t^b) + \pi_t^{H_2} m_t^{H_2,b} - \pi^{ely} - \pi^{gas}\frac{PGT_t^b}{\eta_{GT}} - \pi^{fc}\delta_t^{fc,b} - \pi^w PW_t^b -$$
$$\pi^s PS_t^b - \pi^{bes}(PBC_t^b + PBD_t^b) - \pi^{wc} PWC_t^b - \pi^{sc} PSC_t^b) - \pi_t^g P_t^{grid}) - \mathcal{W}^{co2} \tag{4.2}$$

Subject to $(\forall t \in \mathcal{T}, \forall b \in \mathcal{B}, \forall l \in \mathcal{L})$:

$$\mathcal{W}^{co2} = \pi^{co2}\varepsilon_0 + \sum_{r=1}^{R+1}[\pi^{co2} + (r-1)\Delta_c]\varepsilon_r \tag{4.3}$$

$$\varepsilon_0 \leq 0; 0 \leq \varepsilon_r \leq \chi^{co2}; 1 \leq r \leq R+1 \tag{4.4}$$

$$\varepsilon^{co2,G} - \kappa^{co2,G} + \varepsilon^{co2,GT} - \kappa^{co2,GT} = \sum_{r=0}^{R+1}\varepsilon_r \tag{4.5}$$

$$\varepsilon^{co2,G} = \sum_t \Theta_t^{co2,G} p_t; \quad \varepsilon^{co2,GT} = \sum_{t\in\mathcal{T}}\sum_{b\in\mathcal{B}} \Theta_t^{co2,GT}\frac{PGT_t^b}{\eta_{GT}} \tag{4.6}$$

$$\kappa^{co2,G} = \varrho^{co2}\sum_{t\in\mathcal{T}} PGT_t^b; \kappa^{co2,GT} = \varrho^{co2}\sum_{t\in\mathcal{T}}\sum_{b\in\mathcal{B}}\frac{PGT_t^b}{\eta_{GT}}; \tag{4.7}$$

$$0.8\pi_t^g \leq \pi_t^{R,b} \leq 1.2\pi_t^g; \sum_{t\in\mathcal{T}}\pi_t^{R,b} = \sum_{t,\in\mathcal{T}}\pi_t^g \tag{4.8}$$

$$\begin{aligned} P_t^{inj,b} =& P_t^{grid} + PGT_t^b + PF_t^b + PW_t^b + PS_t^b + PBD_t^b - PBC_t^b - PNFL_t^b - PFL_t^b - Pel_t^b \\ =& P_{base}\sum_{n\in\mathcal{B}} G_{b,n} V_t^n V_t^b \end{aligned} \tag{4.9}$$

$$-\overline{\mathcal{I}}^f \leq \mathcal{I}_t^f \leq \overline{\mathcal{I}}^f \tag{4.10}$$

$$0.95 \leq V_t^b \leq 1.05 \tag{4.11}$$

$$0 \leq PS_t^b \leq PS_t^{avl,b}\overline{PS}^b; \quad 0 \leq PW_t^b \leq PW_t^{avl,b}\overline{PW}^b \tag{4.12}$$

$$PSC_t^b = PS_t^{pu,b}\overline{PS}^b - PS_t^b; \quad PWC_t^b = PW_t^{pu,b}\overline{PW}^b - PW_t^b \tag{4.13}$$

$$\begin{aligned}&\delta_t^{G,b}\underline{PGT}^B \leq PGT_t^b \leq \delta_t^{G,b}\overline{PGT}^b; \quad \underline{P}^{grid} \leq P_t^{grid} \leq \overline{P}^{grid};\\ &\delta_t^{fc,b}\underline{PF}^b \leq PF_t^b \leq \delta_t^{fc,b}\overline{PF}^b\end{aligned} \tag{4.14}$$

$$\underline{Pel}^b \leq Pel_t^b \leq (1-\delta_t^{fc,b})(\overline{Pel}^b - \underline{Pel}^b) + \underline{Pel}^b; \tag{4.15}$$

$$EB_t^b = EB_{(t-1)}^b + PBC_t^b\eta_{bc} - \frac{PBD_t^b}{\eta_{bd}} \tag{4.16}$$

$$\begin{aligned}&0 \leq PBC_t^b \leq \delta_t^{bat,c,b}\overline{PBC}^b; \delta_t^{bat,c,b} \in \{0,1\}\\ &0 \leq PBD_t^b \leq (1-\delta_t^{bat,c,b})\overline{PBD}^b\end{aligned} \tag{4.17}$$

$$0.2\overline{EB}^b \leq EB_t^b \leq \overline{EB}^t; EB_0^b = EB_T^b \tag{4.18}$$

$$\theta_t^{el,b} = \theta_{t-1}^{el,b} + \frac{(1-\eta_{el})Pel_t^b - \frac{\theta_t^{el,b}-\theta_t^{am}}{R_{heat}^{EL}} - hr_t^b}{C_{lmp}^{el}} \tag{4.19}$$

$$60^\circ C \leq \theta_{t,b}^{el} \leq 80^\circ C; \theta_{0,b}^{el} = 70^\circ C \tag{4.20}$$

$$VH_{t,b} = VH_{t-1,b} + \frac{\eta_{el}\left(\frac{Pel_t^b}{Q_{hhv}^{H_2}}\right) - \frac{PF_t^b}{Q_{hhv}^{H_2}} - m_t^{H_2,d,b}}{\varrho_{H_2}} \tag{4.21}$$

$$\underline{VH}^b \leq VH_t^b \leq \overline{VH}_t^b; VH_0^b = VH_T^b \tag{4.22}$$

$$PFL_t^b = \begin{cases} \sum_{e,b}(PEV_{t,e}^{C,b} - PEV_{t,e}^{D,b}) + \sum_{a,b} PA_{t,a}^b : \forall t \in \mathcal{T}^{a,e} \\ \sum_{a,b} PA_{t,a}^b : \forall t \in \mathcal{T} \setminus \mathcal{T}^{a,e} \end{cases} \tag{4.23}$$

$$PFL_t^b \geq 0: \quad \forall t \in \mathcal{T} \tag{4.24}$$

The first and second terms in (4.2) denote income from electricity sale, while the third term denotes income from H_2 sale. The costs of operating P2H, GT, FC, WPG, SPG, and BESS are given by the fourth, fifth, sixth, seventh, eighth, and ninth terms, respectively. The tenth, eleventh, twelfth, and thirteenth terms are WPG and SPG power curtailment and grid power costs, respectively. The last term of eq. (4.2) denotes the

carbon trading cost of the DCμG. Carbon production is due to the power procured from the upstream grid and power produced by the GT. A ladder-type carbon trading model is adopted in this work. The carbon price increases from the base carbon price in intervals when the carbon emission exceeds the free carbon quota [204]. The ladder-type carbon trading model is expressed by (4.3)-(4.7) [204]. (4.8) specifies that the RPP should lie between 80% and 120% of the day-ahead power price of the primary grid, but the average RPP in a day should equal the average day-ahead energy price of the upstream grid. The nodal power balance equation is given by (4.9). (4.10) and (4.11) show the feeder current and bus voltage limits, respectively. RES generation and curtailment constraints are given in (4.12) and (4.13), respectively. The rating constraint of the controllable units, including the GIC, is given by (4.14). Power constraints of the P2H unit are given by (4.15). The BESS constraints are given by (4.16) (energy update), (4.17) (charging and discharging power constraints), and (4.18) (DOC and DOD constraints). The electrolyzer stack temperature and their limits are shown in (4.19) and (4.20), respectively. The H_2 volume in the HSS and corresponding constraints are given by (4.21) and (4.22), respectively. The total flexible load at a bus is due to PHEVs and TCLs connected to the bus (4.23), which should be non-negative (4.24).

4.2.3.2 Islanding constraints for the upper-level problem

Including islanding constraint in the EMS of grid-connected DCμG guarantees secure operation in the event of unintended islanding. A $24-1$ islanding criterion is used in this work, in which 24 denotes the scheduling horizon (i.e., 24 hours) and 1 denotes the consecutive hours for which the DCμG can operate in island mode [205]. In other words, the islanding can occur at any time in the scheduling horizon, and the DCμG should operate securely in the islanded mode for one hour after islanding takes place. Further, the EMS is designed to not allow load curtailment within one hour of the islanding event. If the DCμG is not reconnected to the upstream grid within the mentioned time frame, then EMS for island operating mode is activated, and load curtailment is allowed if necessary.

Islanding constraints are given by (4.25)-(4.31). The loss of the main grid power due to unintentional islanding can be compensated by increasing the generation of controllable sources like the FC and GT and reducing the power consumption of the electrolyzer

without violating the power rating constraints of the FC, GT, and the electrolyzer (4.25). If the BESS is in discharging mode before islanding, then the BESS can compensate for the loss of the main grid power by increasing the discharging power (4.26). On the other hand, if the BESS is charging before the islanding event, then the BESS should reduce the charging power or stop charging and switch over to discharging mode (4.26). The BESS DOC and DOD constraints should not be violated after islanding when the BESS deploys the islanding reserve (4.27). Similarly, the volume constraints of the HSS should not be violated when the islanding reserve is activated by the FC and the electrolyzer (4.28). When the islanding reserves are activated, the nodal power balance is given in (4.29) ($P_t^{grid} = 0$). Also, the feeder currents and bus voltages should be within limits when the islanding reserves are activated ((4.30) and (4.31)).

$$\begin{aligned} &0 \leq PGT_t^{b,i}; 0 \leq PF_t^{b,i}; 0 \leq Pel_t^{b,r}; Pel_t^b - Pel_t^{b,r} \geq \underline{Pel}^b \\ &PGT_t^b + PGT_t^{b,i} \leq \delta_t^{G,b}\overline{PGT}^b; PF_t^b + PF_t^{b,i} \leq \delta_t^{fc,b}\overline{PF}^b; \end{aligned} \tag{4.25}$$

$$\begin{aligned} &0 \leq PBC_t^{b,r} \leq PBC_t^b; \quad PBC_t^b - PBC_t^{b,r} \leq \delta_t^{bat,c,I,b}\overline{PB^b} \\ &0 \leq PBD_t^{b,i} \leq (1 - \delta_t^{bat,c,I,b})\overline{PB^b} - PBD_t^b; \delta_t^{bat,c,I,b} \in \{0,1\} \end{aligned} \tag{4.26}$$

$$\underline{EB}^b \leq EB_{t-1}^b + (PBC_t^b - PBC_t^{b,r})\eta_{bc} - \frac{PBD_t^b + PBD_t^{b,i}}{\eta_{bd}} \leq \overline{EB}^b \tag{4.27}$$

$$\underline{VH}^b \leq VH_{t-1}^b + \frac{\frac{\eta_{el}(Pel_t^b - Pel_t^{b,r}) - (PF_t^b + PF_t^{b,i})}{Q_{hhv}^{H_2}} - m_{t,b}^{H_2}}{\varrho_{H_2}} \leq \overline{VH}^b \tag{4.28}$$

$$\begin{aligned} P_t^{inj,I,b} &= PGT_t^b + PGT_t^{b,i} + PF_t^b + PF_t^{b,i} + PW_t^b + PS_t^b + PBD_t^b + PBD_t^{b,i} - \\ &(PBC_t^b - PBC_t^{b,r}) - PNFL_t^b - PFL_t^b - (Pel_t^b - Pel_t^{b,r}) \\ &= P_{base} \sum_{n \in \mathcal{B}} G_{b,n} V_t^{I,n} V_t^{I,b} \end{aligned} \tag{4.29}$$

$$-\overline{\mathcal{I}}^f \leq \mathcal{I}_t^{f,I} \leq \overline{\mathcal{I}}^f \tag{4.30}$$

$$0.95 \leq V_t^{b,I} \leq 1.05 \tag{4.31}$$

4.2.3.3 Lower-level problem

The lower-level problem for consumers is as follows:

$$\min \mathcal{W}_{2b}; \mathcal{W}_{2b} = \sum_{t\in\mathcal{T}}\sum_{b\in\mathcal{B}} \pi_t^{R,b} PFL_t^b = \sum_{t\in\mathcal{T}}\sum_{a} \pi_t^{R,b} PA_{t,a}^b + \sum_{t\in\mathcal{T}^{a,v}}\sum_{v,b} \pi_t^{R,b}(PEV_{t,v}^{C,b} - PEV_{t,v}^{D,b}) \tag{4.32}$$

Subject to ($\forall t \in \mathcal{T}, \forall b \in \mathcal{B}, \forall v \in \mathcal{V}, \forall a \in \mathcal{A}$):

$$\begin{aligned} &0 \leq PEV_{t,v}^{C,b} \leq \overline{PEV}_v^C : \forall t \in \mathcal{T}^{a,v}; PEV_{t,v}^C = 0 : \forall t \notin \mathcal{T}^{a,v} \\ &0 \leq PEV_{t,v}^{D,b} \leq \overline{PEV}_v^D : \forall t \in \mathcal{T}^{a,v}; PEV_{t,v}^D = 0 : \forall t \notin \mathcal{T}^{a,v} \end{aligned} \tag{4.33}$$

$$E_{t,v}^E = \begin{cases} E_v^{AE} + PEV_{t,v}^C \eta_{ev}^c - \frac{PEV_{t,v}^D}{\eta_{ev}^D} : t = t_{a,v} \\ E_{(t-1),v}^E + PEV_{t,v}^C \eta_{ev}^c - \frac{PEV_{t,v}^D}{\eta_{ev}^D} : \forall t \in \mathcal{T}^{a,v} \setminus t_{a,v} \end{cases} \tag{4.34}$$

$$\begin{cases} \underline{E}_v^E \leq E_{t,v}^E \leq \overline{E}_v^E : \forall t \in \mathcal{T}^{a,v} \setminus t_{d,v} \\ E_{t,v}^E = E_v^{E,R} : t = t_{d,v} \end{cases} \tag{4.35}$$

$$\theta_{t,a}^{A,b} = \epsilon_A \theta_{(t-1),a}^{A,b} + (1-\epsilon_A)\left(F_t - \frac{\eta_A\, PA_{t,a}^b}{A_a^{cond,b}}\right) \tag{4.36}$$

$$\begin{cases} \underline{\theta}_a^{A,b} \leq \theta_{t,a}^{A,b} \leq \overline{\theta}_a^{A,b} : \forall t \in \mathcal{T}; \theta_{T,a}^{A,b} = \theta^{des} \end{cases} \tag{4.37}$$

$$0 \leq PA_{t,a}^b \leq \overline{PA}_a^b : \forall t \in \mathcal{T} \tag{4.38}$$

PHEV constraints are given by (4.33) (charging and discharging power constraints), (4.34) (energy update), (4.35) (DOC and DOD constraints). The indoor temperature of the smart home cooled by the air con considering the thermal inertia is given in (4.36). The indoor temperature and power constraints of the air con are given by (4.37) and (4.38), respectively.

4.2.4 Solution methodology

4.2.4.1 Convex approximation of non-convex DCμG network model using linearisation technique

Due to the non-affine equality constraint eq. (4.9), the network model becomes non-convex [156]. The convexification of non-affine equality constraints is done using linearisation.

The upstream grid is connected to DCμG at bus #1 using a GIC. Also, the bus voltage of bus #1 (i.e., the bus to which the GIC is connected) is maintained at 1.0 p.u.. Therefore, bus #1 is considered as a slack node [182]. Under normal operation, voltages (V_t^b) are close to 1.0 p.u.. We can write the following:

$$V_t^b = 1 + \Delta V_t^b; V_t^n = 1 + \Delta V_t^n; \quad \Delta V_t^b, \Delta V_t^n << 1 \tag{4.39}$$

Therefore, eq. (4.9) can be rewritten as:

$$\begin{aligned} \frac{P_t^{inj,b}}{P_{base}} &= \sum_{n\in\mathcal{B}} G_{b,n} V_t^n V_t^b = \sum_{n\in\mathcal{B}} G_{b,n}(1+\Delta V_t^b)(1+\Delta V_t^b) \\ &= \sum_{n\in\mathcal{B}} G_{b,n}(1+\Delta V_t^n + \Delta V_t^b + \Delta V_t^b \Delta V_t^b) \approx \sum_{n\in\mathcal{B}} G_{b,n}(1+\Delta V_t^n + \Delta V_t^b) \end{aligned} \tag{4.40}$$

The product $\Delta V_t^b \Delta V_t^n$ can be neglected in eq. (4.40), since ΔV_t^n and ΔV_t^b are small. Using eq. (4.39) in eq. (4.40), we obtain:

$$\frac{P_t^{inj,b}}{P_{base}} \approx \sum_{n\in\mathcal{B}} G_{b,n}(V_t^n + V_t^b - 1) = \sum_{n\in\mathcal{B}} G_{b,n} V_t^n = \sum_{n\in\mathcal{B}} G_{b,n} \Delta V_t^n \tag{4.41}$$

Using the symmetry property of G bus in eq. (4.41), we can write $\sum_{n\in\mathcal{B}} G_{b,n} = 0$ and $\sum_{n\in\mathcal{B}} G_{b,n} V_t^b = 0$. Therefore, the non-convex nodal power balance equality constraint of eq. (4.9) can be replaced by the linear power flow model given by eq. (4.41). In the matrix form, we can write:

$$[\mathbf{p}_t^{inj}] = P_{base}[\mathbf{G}][\mathbf{\Delta V}_t] \tag{4.42}$$

Slack bus row and column are removed to obtain an invertible matrix $[\mathbf{G}_{mod}]$ (as $[\mathbf{G}]$ is a singular matrix). Also, from the power injection column, the row corresponding to the slack bus is removed to form $\mathbf{p}_t^{inj,mod}$.

$$[\mathbf{\Delta V}_t^{mod}] = \frac{1}{P_{base}}[\mathbf{G}_{mod}]^{-1}[\mathbf{p}_t^{inj,mod}] \tag{4.43}$$

The row and column corresponding to the slack bus, which contains all zero values, are added to the matrix $[\mathbf{G}_{mod}]^{-1}$ to form $\mathcal{G}$. We can write as:

$$[\mathbf{\Delta V}_t] = \frac{1}{p_{bs}}[\mathcal{G}][\mathbf{p}_t^{inj}] \tag{4.44}$$

Voltage deviation (from 1.0 p.u.) at bus #b is given as:

$$\Delta V_t^b = \frac{1}{P_{base}} \sum_{n \in \mathcal{B}} \mathcal{G}_{b,n} P_t^{inj,b} \tag{4.45}$$

To measure the impact of power injection change at bus #j on the line current $\mathcal{I}^f$ of the line #f, GSDF is defined. Therefore, GSDF for line $\#f$ connected between buses $\#b$ and $\#n$ is as follows:

$$GSDF^{f,j} = \Delta \mathcal{I}_t^f / \Delta P_t^{inj,j} \tag{4.46}$$

Where $GSDF^{f,j}$ denotes GSDF (p.u) of the DCμG. The line current in $\#f$ is given by:

$$\mathcal{I}_t^f = (\Delta V_t^b - \Delta V_t^n) g_{b,n}; \quad g_{b,n} = -G_{b,n} \tag{4.47}$$

Substituting $\Delta V_t^b - \Delta V_t^n$ from eq. (4.45) in eq. (4.47), we get:

$$\mathcal{I}_t^f = (\sum_{j \in \mathcal{B}} (\mathcal{G}_{b,j} - \mathcal{G}_{n,j}) P_t^{inj,j}) \frac{g_{b,n}}{P_{base}} \tag{4.48}$$

Therefore, the GSDF from bus $\#j$ to line $\#f$ can be defined as:

$$GSDF_{f,j} = \frac{g_{b,n}(\mathcal{G}_{b,j} - \mathcal{G}_{n,j})}{p_{bs}} = \frac{-G_{b,n}(\mathcal{G}_{b,j} - \mathcal{G}_{n,j})}{P_{base}} \tag{4.49}$$

Therefore, the network constraint, given by eq. (4.10) can be rewritten in linear form as follows:

$$-\overline{\mathcal{I}}^f \leq \sum_{b \in \mathcal{B}} (-G_{b,n}(\mathcal{G}_{b,j} - \mathcal{G}_{n,j})) \left(\frac{P_t^{inj,b}}{P_{base}} \right) \leq \overline{\mathcal{I}}^f; \quad \forall t \in \mathcal{T} \tag{4.50}$$

(4.9) and (4.10) are replaced by (4.41) and (4.50), respectively in the EMS model. Also, (4.29) and (4.30) are replaced by their linear approximations along similar lines.

4.2.4.2 Conversion of bi-level problem to single level

The lower-level problem of flexible consumers is converted to a set of equivalent constraints using KKT conditions and added to the upper-level problem. Therefore, the bi-level problem is converted to a single-level problem. The RPP is determined by the

DCμGO before lower-level consumers decide their optimal strategy. As a result, both upper and lower-level problems are convex problems, and KKT conditions guarantee global optimality. Slack variables are added to convert inequality constraints in (4.33) and (4.35) to equality constraints and we obtain the following first-order KKT conditions ((4.51), (4.52)) and complementary slackness conditions (4.53) for the PHEV power consumption optimisation problem:

$$\pi_t^{R,b} - \lambda_{t,v}^{E,C,-,b} + \lambda_{t,v}^{E,C,+,b} - \eta_{ev}^{c}\lambda_{v}^{E,E,b} + \eta_{ev}^{c} \sum_{\substack{\tau \geq t; \\ \tau \in \mathcal{T}^{a,v} \setminus t_{a,v}}} (\lambda_{\tau,v}^{E,E,+,b} - \lambda_{\tau,v}^{E,E,-,b}) = 0 : \forall t \in \mathcal{T}^{a,v} \tag{4.51}$$

$$-\pi_t^{R,b} - \lambda_{t,v,b}^{E,D,-} + \lambda_{t,v,b}^{E,D,+} + \frac{\lambda_{v}^{E,E,b}}{\eta_{ev}^{D}} - \frac{1}{\eta_{ev}^{D}} \sum_{\substack{\tau \geq t; \\ \tau \in \mathcal{T}^{a,v} \setminus t_{a,v}}} (\lambda_{\tau,v}^{E,E,+,b} - \lambda_{\tau,v}^{E,E,-,b}) = 0 : \forall t \in \mathcal{T}^{a,v} \tag{4.52}$$

$$\begin{aligned}
&\{\varpi_{t,v}^{E,C,+,b}\lambda_{t,v}^{E,C,+,b} = 0; \varpi_{t,v}^{E,C,-,b}\lambda_{t,v}^{E,C,-,b} = 0;\}\forall t \in \mathcal{T}^{a,v} \\
&\{\varpi_{t,v}^{E,D,+,b}\lambda_{t,v}^{E,D,+,b} = 0; \varpi_{t,v}^{E,D,-,b}\lambda_{t,v}^{E,D,-,b} = 0;\}\forall t \in \mathcal{T}^{a,v} \\
&\{\varpi_{t,v}^{E,E,+,b}\lambda_{t,v}^{E,E,+,b} = 0; \varpi_{t,v}^{E,E,-,b}\lambda_{t,v}^{E,E,-,b} = 0;\}\forall t \in \mathcal{T}^{a,v} \setminus t_{d,v}
\end{aligned} \tag{4.53}$$

$\lambda_{t,v}^{E,C,+,b}/\lambda_{t,v}^{E,C,-,b}/\lambda_{t,v}^{E,D,+,b}/\lambda_{t,v}^{E,D,-,b}/\lambda_{\tau,v}^{E,E,+,b}/\lambda_{\tau,v}^{E,E,-,b}/\lambda_{v}^{E,E,b}$ are Lagrange multipliers for PHEV charging power upper/lower limits, PHEV discharging power upper/lower limits, and PHEV energy upper/lower/equality limits, respectively.

$\varpi_{t,v}^{E,C,+,b}/\varpi_{t,v}^{E,C,-,b}/\varpi_{t,v}^{E,D,+,b}/\varpi_{t,v}^{E,D,-,b}/\varpi_{t,v}^{E,E,+,b}/\varpi_{t,v}^{E,E,-,b}$ are the slack variables for PHEV charging power upper/lower limits, discharging power upper/lower limits, and PHEV battery energy upper/lower limits inequalities, respectively

The inequality constraints in (4.37) and (4.38) in the power consumption optimisation problem of the TCL are also converted to equality constraints by adding slack variables. The first order KKT conditions for the TCL (4.54) and complementary slackness conditions (4.55) are as follows:

$$\pi_t^{R,b} + \lambda_{t,a}^{A,P,-} - \lambda_{t,a}^{A,P,+} + (1-\epsilon_A)(\frac{\eta_A}{A_a^{cond,b}})(\lambda_a^{A,\theta,E,b}(\epsilon_A)^{T-t} + \sum_{\substack{\tau \geq t; \\ \tau \in \mathcal{T} \setminus T}} (\epsilon_A)^{\tau-t}(\lambda_{t,a}^{A,\theta,+} + \lambda_{t,a}^{A,\theta,-})) = 0 : \forall t \in \mathcal{T} \tag{4.54}$$

$$\{\varpi_{t,a}^{A,P,+}\lambda_{t,a}^{A,P,+}=0;\varpi_{t,a}^{A,P,-}\lambda_{t,a}^{A,P,-}=0;\}\forall t\in\mathcal{T}\setminus T$$
$$\{\varpi_{t,a}^{A,\theta,+}\lambda_{t,a}^{A,\theta,+}=0;\varpi_{t,a}^{A,\theta,-}\lambda_{t,a}^{A,\theta,-}=0;\}\forall t\in\mathcal{T}\setminus T \tag{4.55}$$

$\lambda_{t,a}^{A,P,+}/\lambda_{t,a}^{A,P,-}/\lambda_{t,a}^{A,\theta,+}/\lambda_{t,a}^{A,\theta,-}/\lambda_{a,b}^{A,\theta,E}$ are Lagrange multipliers for air con power upper/lower limits, and indoor temperature upper/lower/equality limit constraints, respectively.

$\varpi_{t,a}^{A,P,+}/\varpi_{t,a}^{A,P,-}/\varpi_{t,a}^{A,\theta,+}/\varpi_{t,a}^{A,\theta,-}$ are the slack variables for indoor temperature upper/lower limits, and air con power upper/lower limit inequalities, respectively.

Since all inequality constraints in the lower-level problem are converted to equality constraints by slack variable formulations, there are no sign restrictions on the Lagrange multipliers. The non-convex slackness conditions are linearised by the big-M approach [206]. The lower level problem is a Linear programming (LP) problem. Following the "strong duality theorem" of LP, if the dual problem has optima, then the objective value of the dual problem is equal to the objective value of the primal problem [206]. Therefore, dual of the objective of the lower-level problem is used to replace the bilinear terms of the upper-level problem with the following ((4.56) and (4.57)) substitutions:

$$\sum_{t\in\Omega^{a,v}}\pi_t^{R,b}(PEV_{t,v}^{C,b}-PEV_{t,v}^{D,b})=\sum_{t\in\mathcal{T}^{a,v}\setminus t_{d,v}}((\overline{E}_v^E-E_v^{AE})\lambda_{t,v}^{E,E,+,b}+(E_v^{AE}-\underline{E}_v^E)\lambda_{t,v}^{E,E,-,b})+$$
$$(E_v^{E,R}-E_{0,v}^{AE})\lambda_v^{E,E,b}+\sum_{t\in\mathcal{T}^{a,v}}(\lambda_{t,v}^{E,C,+,b}\overline{PEV}_v^C+\lambda_{t,v}^{E,D,+,b}\overline{PEV}_v^D) \tag{4.56}$$

$$\sum_{t\in\mathcal{T}}\pi_t^{R,b}PA_{t,a}^b=\frac{A_{a,b}^{cond}}{\eta_A(\epsilon_A-1)}(\sum_{t\in\mathcal{T}\setminus T}(\lambda_{t,a}^{A,\theta,+}(\overline{\theta}_a^{A,b}-\epsilon_A^{(t)}\theta_{0,a}^{A,b}-(1-\epsilon_A)(\sum_{\tau=1}^{\tau\le t}\theta_{\tau,a}^b\epsilon_A^{(t-\tau)}))-\lambda_{t,a}^{A,\theta,-,b}(\epsilon_A^{(t)}\theta_{0,a}^{A-,b}$$
$$\underline{\theta}_a^{A,b}+(1-\epsilon_A)(\sum_{\tau=1}^{\tau\le t}\theta_{\tau,a}^b\epsilon_A^{(t-\tau)})))-\lambda_a^{A,\theta,E,b}(\epsilon_A^{(T)}\theta_{0,a}^{A-,b}\underline{\theta}_a^{A,b}+(1-\epsilon_A)(\sum_{\tau=1}^{\tau\le T}\theta_{\tau,a}^b\epsilon_A^{(t-\tau)})))-$$
$$\sum_{t\in\mathcal{T}}\lambda_{t,a}^{A,P,+,b}\overline{PA}_a^b \tag{4.57}$$

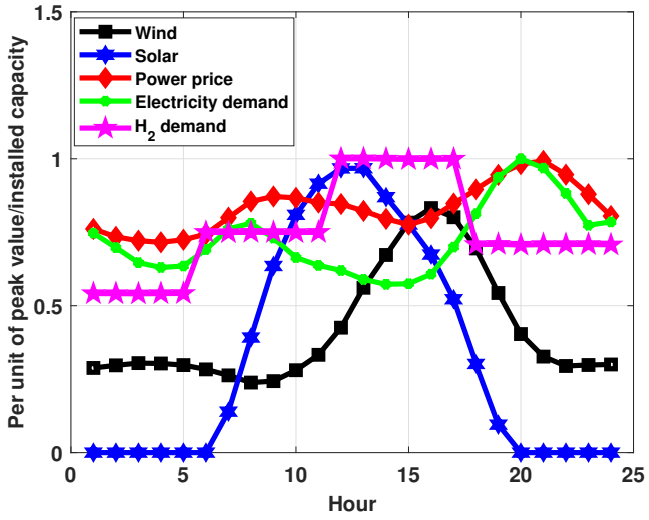

Figure 4.3: Hourly generation, demand, and price profile

4.2.4.3 Existence of SG equilibrium

Following are the conditions for the existence of an equilibrium in the SG: (a) The DCμGO profit is a continuous and nonempty function of strategy sets of the DCμGO and flexible consumers; (b) The energy usage cost of flexible consumers is a continuous and nonempty function of strategy sets of the DCμGO and flexible consumers.; (c) The energy usage cost of flexible consumers is a concave function of the strategy sets of flexible consumers.

Proof: $\hat{\mathcal{W}}_1$ and $\mathcal{W}_{2b}$ are continuous and nonempty functions of $\pi_t^{R,b}$, PFL_t^b. Also, $\frac{\partial^2 \mathcal{W}_{2b}}{\partial (PFL_t^b)^2} = 0$. Therefore, $\mathcal{W}_{2b}$ is concave in PFL_t^b. Hence, the equilibrium exists.

4.2.4.4 Uniqueness of SG equilibrium

Following are the conditions for the uniqueness of the SG equilibrium: (a) Given a strategy of the flexible consumers, the profit of the DCμGO should have a unique maximum value; (b) Given a strategy of the DCμGO, the energy usage cost of flexible consumers should have a unique minimum value.

Proof: $\frac{\partial \hat{\mathcal{W}}_1}{\partial \pi_t^{R,b}} = PFL_t^b > 0$. The above implies that $\hat{\mathcal{W}}_1$ (DCμGO profit) is an increasing function of $\pi_t^{R,b}$ having a unique maximum in the definition domain. Also, $\frac{\partial \mathcal{W}_{2b}}{\partial PFL_t^b} = \pi_t^{R,b} > 0$ (energy usage cost of flexible consumers) is an increasing function of PFL_t^b having a unique minimum in the definition domain. Hence, the proof.

Table 4.2: Test System Data

GIC:	Bus #1, $\underline{P^{grid}} = 0kW$, $\overline{P^{grid}} = 50kW$;
BESS:	Bus #2, $\eta_{bc}/\eta_{bd} = 95\%$, $\underline{PBC} = 0kW$, $\overline{PBC} = 15kW$ $\underline{PBD} = 0kW$, $\overline{PBD} = 15kW$, $\underline{EB} = 6kWh$, $\overline{EB} = 30kWh$ $EB_0 = 18kWh$, $\pi^{bes} = 0.006\$/kWh$;
FC [78]:	Bus #3, $\underline{PF} = 5kW$, $\overline{PF} = 50kW$, $\pi^{fc} = 0.133\$/kWh$;
Electrolyzer/P2H & HSS[78]:	Bus #3, $\underline{Pel} = 6.5kW$, $\overline{Pel} = 150kW$, $\pi^{ely} = 0.107\$$ $\eta_{el} = 0.68$, $\varrho_{H_2} = 7.8kg/m^3$, $R^{EL}_{heat} = 18°C/kW$, $C^{el}_{lmp} = 0.0833MW/°C$, $Q^{H_2}_{hhv} = 39.4kWh/kg$, $\underline{VH} = 0.25Nm^3$, $\overline{VH} = 1.5Nm^3$, $VH_0 = 0.9Nm^3$, $\pi^{H_2} = 5\$/kg$;
WPG:	Bus #3, $\overline{PW} = 100kW$, $\pi^{wc} = 0.2\$/kW$, $\pi^{w} = 0.0342\$/kW$;
SPG:	Bus #3, $\overline{PS} = 100kW$, $\pi^{sc} = 0.2\$/kW$, $\pi^{s} = 0.0274\$/kW$;
GT [204]:	Bus #6, $\overline{PGT} = 30kW$, $\underline{PGT} = 3kW$, $\eta_{GT} = 0.35$, $\pi^{gas} = 0.0565\$/100lb$;
TCL parameters [184]:	$\epsilon_A = 0.93$, $\eta_A = 2.5$, $\overline{PA} = 3.5kW$, $\underline{\theta}^A_a = 75.20°F$, $\overline{\theta}^A_a = 80.6°F$, $\theta^A_{0,a} = 77°F$;
Line ratings:	$\overline{\mathcal{I}}_l = 0.2$ p.u;
Non-flexible loads:	$\max_t\{PNFL^4_t\} = 25$kW, $\max_t\{PNFL^5_t\} = 50$kW;
PHEV:	$\eta^C_{ev}/\eta^D_{ev} = 95\%$;
Carbon Trading parameters [204]:	$\varrho^{co2} = 0.648kgCO_2/kWh$, $\chi^{co2} = 10kgCO_2$, $\pi^{co2} = 0.014\$/kgCO_2$, $\Delta_c = 0.0035\$/kgCO_2$;

4.3 Numerical studies

4.3.1 Test system and simulation tool

A modified version of the six-bus DCμG test system network reported in [61] is adopted. The voltage and power bases are 380 V and 250 kW, respectively. The line parameters are given in [61]. The flexible and non-flexible loads are connected to buses #4 and

#5. Locations, sizes, and parameters of GIC, RES, BESS, HSS, P2H, H2P, and GT units are given in table 4.2. Parameters of flexible loads and carbon trading are given in table 4.2. The maximum day-ahead energy price is 0.173$/kWh, and the maximum H_2 demand in a day is 0.7427 kg. The carbon intensities of the upstream grid and gas port are adopted from [204]. The maximum likelihood values of input RVs are shown in fig. 4.3. The maximum likelihood values are generated using the Copula-embedded Monte Carlo simulation technique considering correlated and uncorrelated input RV uncertainties (explained in section 4.2.2) to minimise the risk of dispatch strategy. The PHEV driving parameters are taken from [173]. The codes are written on a desktop with Intel(R) Core(TM) $i7-9700CPU@3.00GHz$ and 16.0 GB RAM. Codes are written in MATLAB R2023a with the YALMIP toolbox and GUROBI solver.

4.3.2 Simulation results

We have considered three optimisation modes. In mode 1, an independent optimisation of the DCμGO is done considering islanding constraints and DR participation. In other words, a single-level optimisation is done to maximise the profit of the DCμGO. In mode 2, the SG-based joint optimisation of DCμGO and flexible consumers is done to achieve a trade-off between DCμGO and flexible consumer objectives. In mode 3, the power consumption pattern of the flexible consumers is first optimised considering day-ahead energy price followed by independent optimisation of the DCμGO objective. In other words, the priority is to minimise the energy consumption cost of the flexible consumers followed by maximisation of the DCμGO profit. Islanding constraints are considered in Mode 2 and Mode 3. The chapter proposes and adopts mode 2 (joint optimisation). Other optimisation modes are for comparison.

4.3.2.1 Study of three optimisation modes

The results are given in table 4.3. The objective in mode 1 is solely to maximise the profit of the DCμGO. Therefore, the profit of the DCμGO is the highest (143.37 $/day) in mode 1 optimisation. However, the cost of electricity use by consumers is the highest (217.67 $/day) in mode 1 optimisation since the interest of the consumers is not considered in the optimisation problem. On the other hand, the priority in mode 3 optimisation is to minimise the electricity usage cost of consumers. Therefore, the electricity usage cost of

Table 4.3: Operating economics of optimisation modes

	DCμGO profit ($/day)	**Electricity usage cost of flexible consumers ($/day)**	**Electricity usage cost of all consumers ($/day)**
Mode 1	143.37	24.39	217.67
Mode 2	**138.55**	**17.30**	**209.65**
Mode 3	135.73	15.64	206.01

Table 4.4: Impact of Islanding Constraints: Mode 2

Entity	**Performance Index**	**Scenarios**	
		$S\#1$	$S\#2$
DCμG	**Income from elec sales ($/day)**	209.61	209.65
	Income from H2 sales ($/day)	67.41	67.41
	Operating cost ($/day)	135.45	138.51
	Profit ($/day)	141.57	138.55
Consumer	**Consumer elec cost ($/day)**	209.61	209.65

the consumers is the least (206.01 $/day) in mode 3 optimisation. However, the profit of the DCμGO is also the least (135.73 $/day) in mode 3. Therefore, mode 1 and mode 2 optimisations prioritise the interests of the DCμGO and the consumers, respectively. From the results summarised in table 4.3, we observe that the profit of the DCμGO (138.55 $/day) and the cost of electricity use of the consumers (209.65 $/day) in mode 2 (joint) optimisation are midway between the figures obtained in mode 1 and mode 3 optimisation. In other words, the proposed approach achieves SG equilibrium with a trade-off between the interests of the DCμGO and the consumers through an interactive decision-making approach in a multi-stakeholder problem. Note that scheduling strategies involving DR implementation in [21, 24, 30, 40, 104] had only considered the interest of the DCμGO and not of the DR participants. Therefore, the mode 2 optimisation proposed in this chapter addresses the limitations of previous studies.

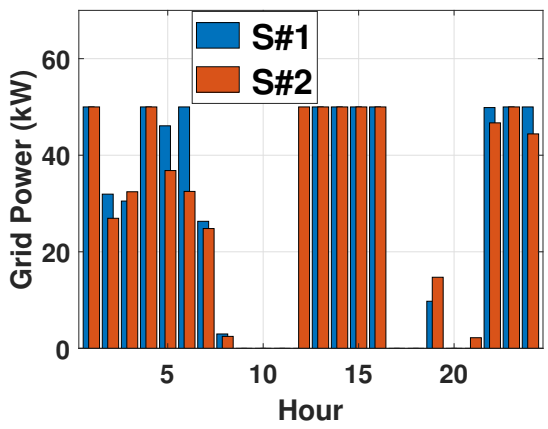

(a) Grid power

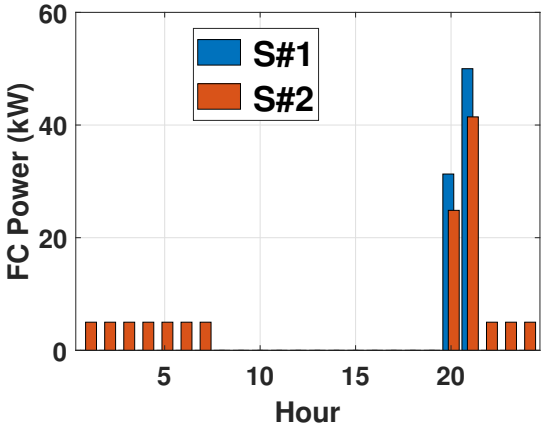

(b) FC power

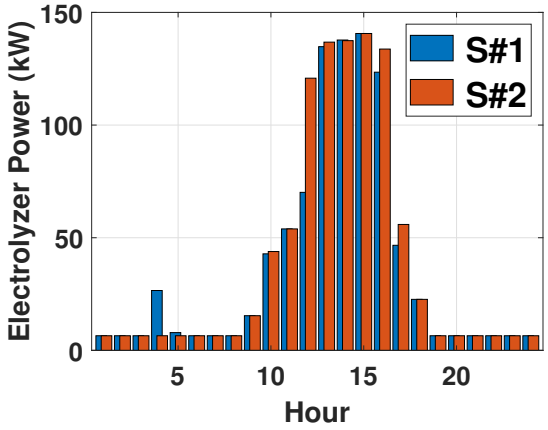

(c) P2H power

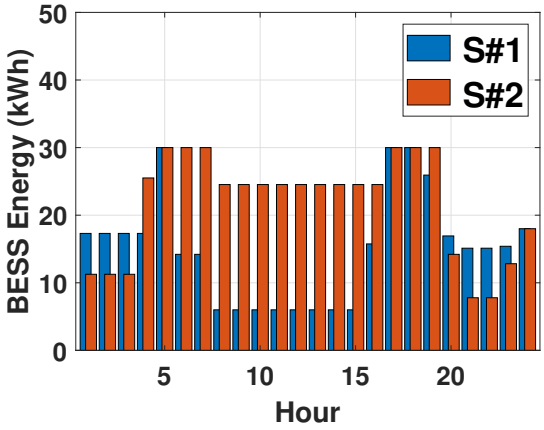

(d) BESS Energy

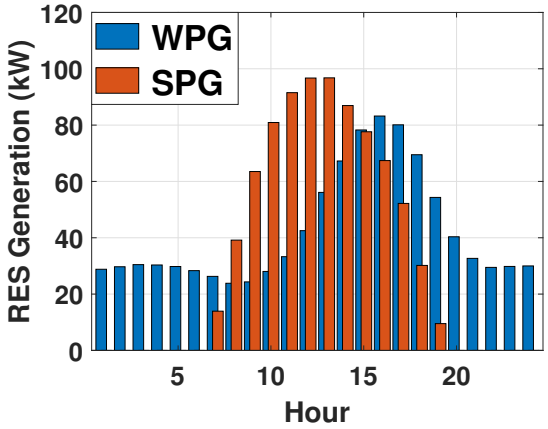

(e) RES generation in S#1 and S#2

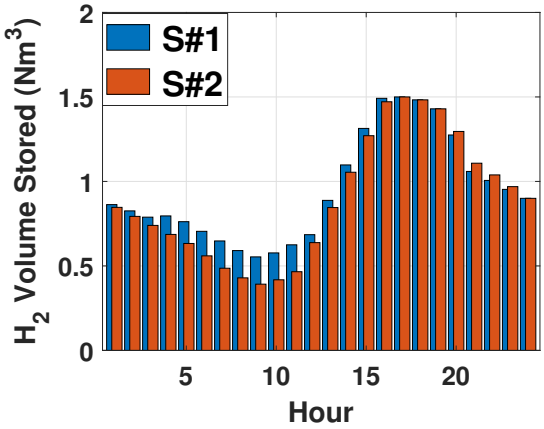

(f) Volume of H_2 in HSS

Figure 4.4: Optimal schedules-Mode 2

4.3.2.2 Impact of islanding constraints on operating economy in mode 2 optimisation

We have considered two different EMS scenarios in mode 2 optimisation to assess the impact of islanding constraints on the operating economy. The islanding constraints are

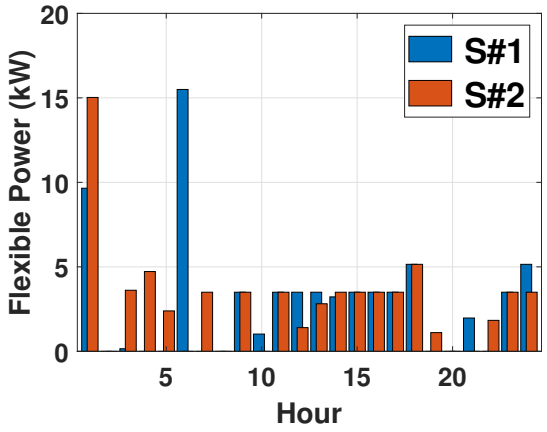

(a) Flexible load power at bus#4

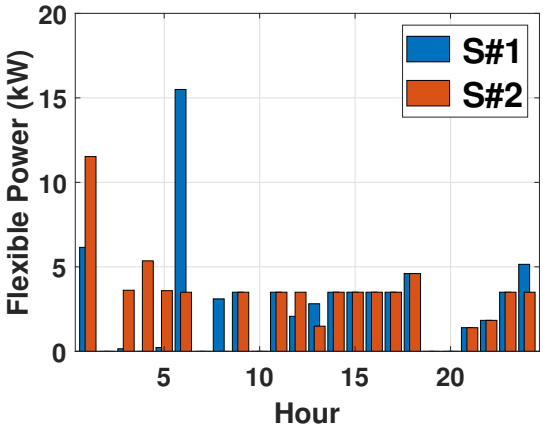

(b) Flexible load power at bus#5

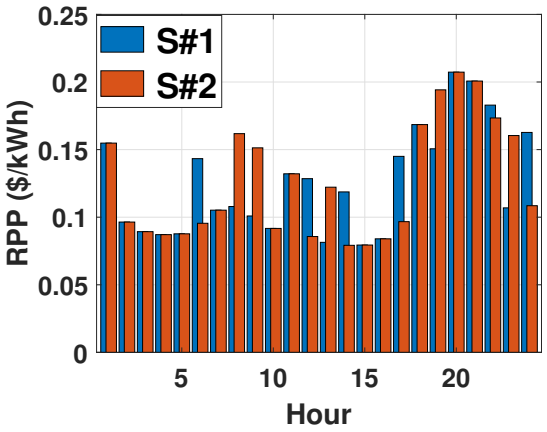

(c) RPP at bus#4

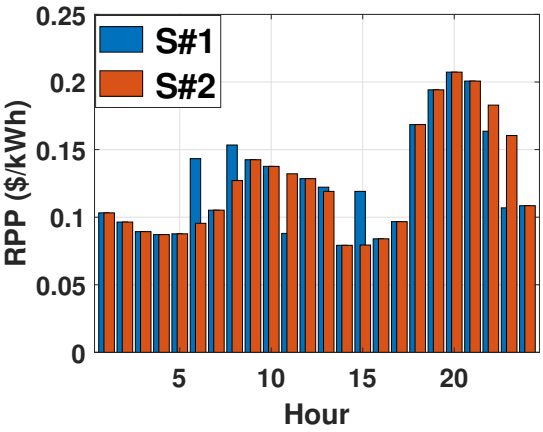

(d) RPP at bus#5

Figure 4.5: Optimal schedules for Flexible load and RPP -Mode 2

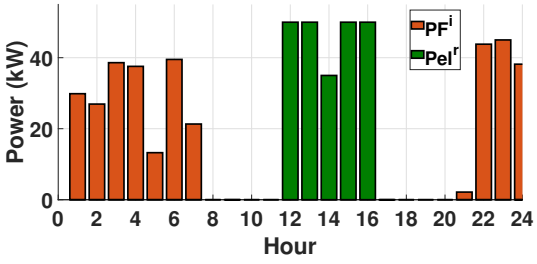

(a) Islanding reserves available from FC and electrolyzer

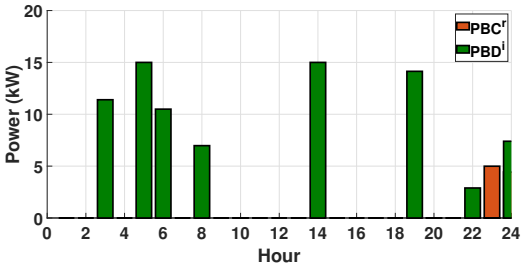

(b) Islanding reserves available from BESS

Figure 4.6: Islanding Reserves in Scenario S#2-Mode 2

not considered in scenario S#1, while islanding constraints are incorporated in scenario S#2. The results are given in table 4.4. Including the islanding constraints reduces the DCμGO profit by $\sim$ 2.13% and increases the DCμGO operating cost by $\sim$ 2.26%. The

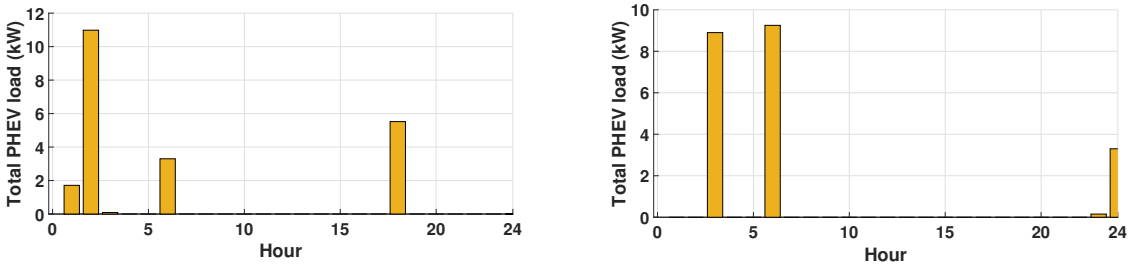

(a) Scenario S#1 (b) Scenario S#2

Figure 4.7: PHEV charging power demand at each load bus-Mode 2

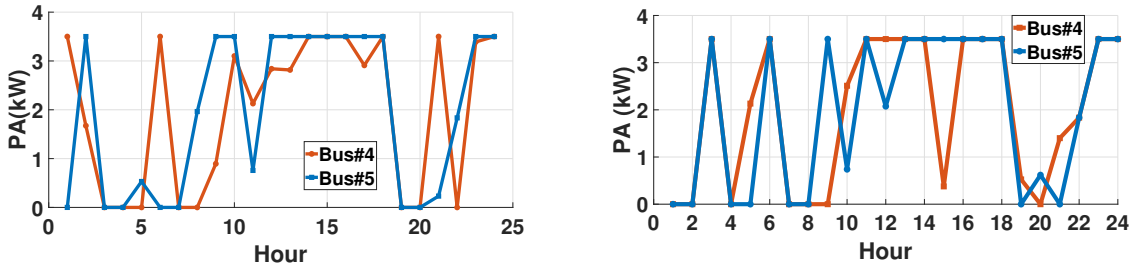

(a) Scenario S#1 (b) Scenario S#2

Figure 4.8: Optimal hourly set points of air con/TCL power-Mode 2

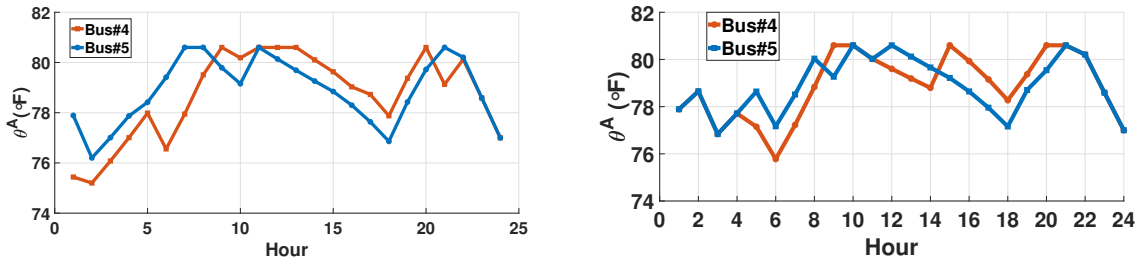

(a) Scenario S#1 (b) Scenario S#2

Figure 4.9: Hourly indoor temperature of a room cooled by TCL-Mode 2

increase in the operating cost of the DCμGO is attributable to the participation of FC and BESS in the islanding reserves. As illustrated in fig. 4.4b, the FC operates at its minimum capacity to provide islanding reserves. The P2H unit also contributes to the islanding reserves, as shown in fig. 4.6a. The BESS does not discharge to its DOD limits and provides islanding reserves during hours #1-#5 (see fig. 4.4d and fig. 4.6b). In other words, setpoints of the DERs in scenario S#2 deviate from the optimal setpoints obtained from purely economic considerations (i.e., S#1) for incorporating islanding capability in the DCμG. As a result, the operating cost increases and the profit of the DCμGO reduces.

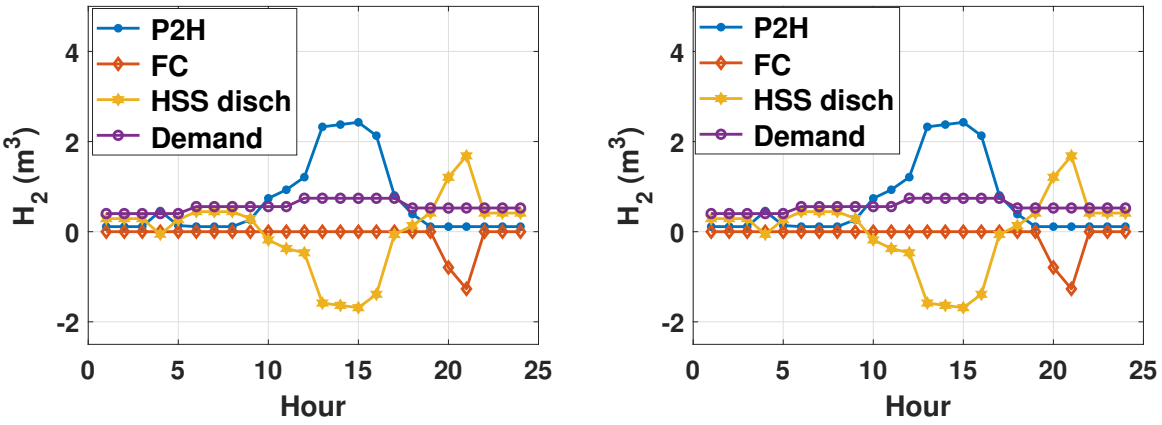

(a) H_2 production and demand S#1 (b) H_2 production and demand S#2

Figure 4.10: H_2 production -Mode 2

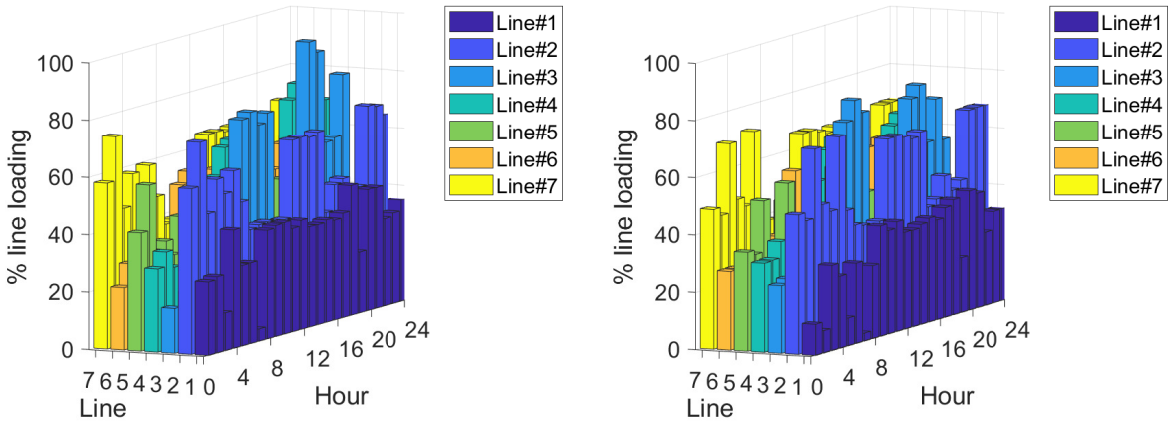

(a) % line loading-Scenario S#1 (b) % line loading-Scenario S#2

Figure 4.11: Hourly line loading-Mode 2

4.3.2.3 Analysis of scenarios S#1 and S#2 in mode 2 optimisation

The optimal power profiles, flexible load, and RPP for scenarios S#1 and S#2 in mode 2 optimisation are shown in fig. 4.4 and fig. 4.5. fig. 4.6 shows the islanding reserve capacities available from various DER. fig. 4.7 shows the optimal PHEV power requirement after DR implementation. fig. 4.8 and fig. 4.9, respectively, show the optimal power setpoints of the TCL and the indoor temperature of a room cooled by the TCL after DR implementation. The day-ahead energy price is relatively low during hours #1−#5 (see fig. 4.3). Therefore, the DCμG purchases power from the upstream grid to meet its load demand (see fig. 4.4a). The FC remains off in scenario S#1 since purchasing power from the upstream grid is

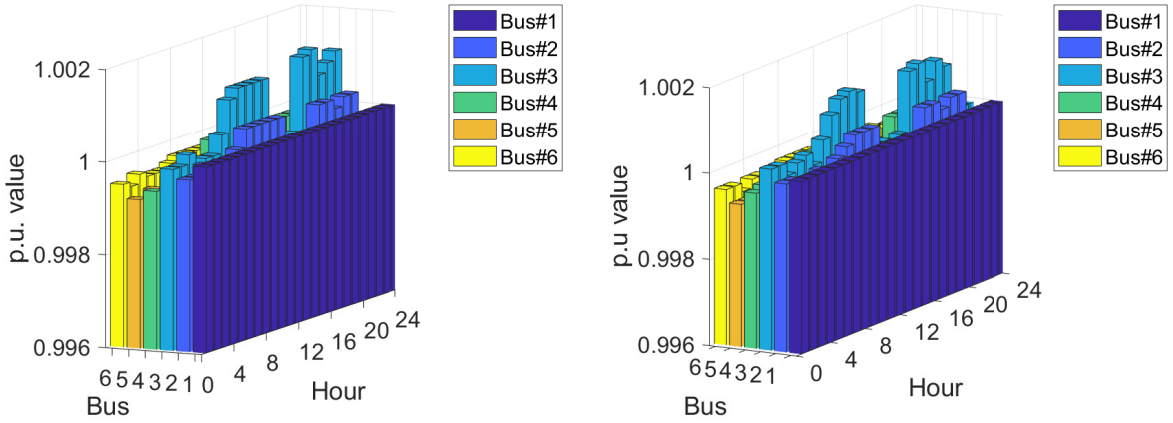

(a) Bus voltage-Scenario S#1 (b) Bus voltage-Scenario S#2

Figure 4.12: Hourly bus voltages-Mode 2

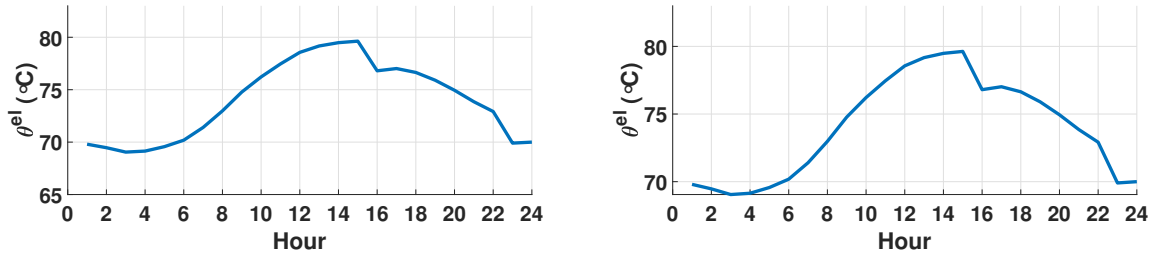

(a) Electrolyzer temperature for Scenario S#1 (b) Electrolyzer temperature for Scenario S#2

Figure 4.13: Hourly temperature of electrolyzer stack-Mode 2

more economical than using FC to generate power. However, in scenario S#2, the FC is on and operates at the minimum rating of 5 kW to provide islanding reserves. This results in an increased operating cost in scenario S#2. fig. 4.6a shows the islanding reserve capacity available from the FC. During hours $\#1-\#5$, the BESS charges to the full capacity of 30 kWh in scenarios S#1 and S#2 since the electricity price in the wholesale market is low (see fig. 4.4d). The RES generation during hours $\#1-\#5$ is due to WPG (fig. 4.4e). Since the non-flexible power demand and day-ahead energy price are low during hours $\#1-\#5$, flexible consumers are encouraged to shift their consumption to this period by setting a low value of RPP (fig. 4.5c, fig. 4.5d, fig. 4.5a, and fig. 4.5b). Therefore, the PHEV charging requirement is met during this period (see fig. 4.7a and fig. 4.7b).The power consumed by the TCLs is shown in fig. 4.8a and fig. 4.8b. The indoor temperature of a room cooled by a TCL remains within the comfort limits of the occupants (see fig. 4.9a and fig. 4.9b). The BESS also provides some islanding reserves in scenario S#2 since

it is not discharged fully up to its DOD limit (see fig. 4.4d and fig. 4.6b). If islanding reserves are to be activated during this period, the FC can increase its generation (see fig. 4.6a), and the BESS can start discharging during hours #3 and #5 (see fig. 4.6b). The H_2 generation, consumption, and demand for scenarios S#1 and S#2 are shown in fig. 4.10. H_2 production by P2H/electrolyzer is represented by positive values, while H_2 consumption by the FC is shown by negative values. During hours $\#1 - \#5$, the H_2 demand is comparatively low and is met by generating H_2 using the P2H unit and discharging the HSS (see fig. 4.10a and fig. 4.10b). The P2H unit consumes a small amount of electricity sufficient to meet the H_2 demand during this period (fig. 4.4c). The H_2 stored in the HSS is more than the minimum storage level to facilitate increased power generation by the FC if the islanding reserve is to be activated (scenario S#2 in fig. 4.4f). Since the P2H unit operates at its minimum power rating during this period in scenario S#2, there is no scope to reduce further its power consumption for providing islanding reserves (see fig. 4.4c). Therefore, the P2H unit cannot provide islanding reserves during this period (see fig. 4.6a).

The grid power price increases during hours $\#6 - \#10$ (fig. 4.3). The non-flexible electricity demand increases from hour #6 to hour #8 and then starts decreasing (fig. 4.3). Since the grid power price is relatively high during this period, the power procurement from the main grid reduces from hour #7 onwards (fig. 4.4a) in both scenarios. The total RES generation increases from hour #7 as the SPG starts generating. Therefore, the dependence on the grid power is reduced. In scenario S#1, the DCμGO does not procure any power from the grid between hours $\#8 - \#10$. In scenario S#2, the DCμGO procures only 6.18 kW from the main grid in hour #8 and does not procure any power from the main grid during hours $\#9 - \#10$. The FC remains off in scenario S#1 during this period (fig. 4.4b). On the other hand, in scenario S#2, the FC remains on (but generates minimum power) during hours $\#6 - \#7$ to provide islanding reserves. The islanding reserves provided by the FC during hours $\#6 - \#7$ are shown in fig. 4.6a. As the dependence on grid power reduces, the FC gets turned off at hour #8 in scenario S#2 (fig. 4.4b) and no longer provides islanding reserves (see fig. 4.6a). In scenario S#1, the BESS discharges between hours $\#6 - \#8$ to meet the load demand (fig. 4.4d). Since the BESS is charged when the grid power price is low and is discharged when the grid power price is higher, an arbitrage benefit is obtained. On the other hand, in scenario

S#2, the power discharged by the BESS is comparatively low, and the energy content of the BESS is higher compared to scenario S#1. The energy content of the BESS can be used to activate islanding reserves if required (fig. 4.4d and fig. 4.6b). The electricity consumption of flexible consumers is also comparatively low during this period in both scenarios (fig. 4.5a, fig. 4.5b, fig. 4.7, fig. 4.8). The P2H unit continues to consume a small amount of electricity to generate a small amount of H_2. The electricity consumption of the P2H unit, and consequently, the H_2 generation, increases from hour #9 onwards in both scenarios. The H_2 demand increases slightly during the period and is catered by discharging the HSS and the H_2 generated by the P2H unit (fig. 4.10a and fig. 4.10b). The discharge of the HSS is slightly higher in scenarios S#2.

The electricity price in the wholesale market and the non-flexible electricity demand reduce between hours #11 and #15 (fig. 4.3). Therefore, the DCμGO imports the maximum possible power (50 kW) from the main grid in both scenarios (fig. 4.4a). The RES generation is also high during this period (fig. 4.4e). The flexible consumer demand during this period is mainly due to cooling requirements (fig. 4.5a, fig. 4.5b, fig. 4.7, fig. 4.8). The FC remains off in both scenarios since the grid power price is low, and the available grid power and RES generation can meet the load demand (fig. 4.4b). Note that the energy content of the BESS is much higher in scenario S#2 (fig. 4.4d) since the BESS and P2H units are important sources of islanding reserves during this period in the absence of the FC (see fig. 4.6a and fig. 4.6b). The excess available generation (from the grid and RES) feeds the P2H unit (fig. 4.4c). Therefore, the H_2 generated by the P2H unit also increases (fig. 4.10a and fig. 4.10b). The generated H_2 not only caters to the H_2 demand but also charges the HSS unit up to the rated volume (fig. 4.10).

The electricity price in the wholesale market and the non-flexible electricity demand increase from hour #16 and are close to peak values during hours $\#19 - \#22$. Consequently, the power procured from the grid decreases in scenarios S#1 and S#2 (fig. 4.4a). The BESS discharges during this period in both scenarios (fig. 4.4d). However, the discharge is lower, i.e., the stored energy is higher after discharge in scenario S#2 to provide sufficient islanding reserves. The P2H power consumption also reduces in both scenarios (fig. 4.4c). The RPP is high (fig. 4.5c and fig. 4.5d), reducing the flexible consumers' consumption in both scenarios (fig. 4.5a, fig. 4.5b, fig. 4.7, fig. 4.8). In both scenarios, the HSS discharges from hour #19 onwards (fig. 4.10a and fig. 4.10b). A part of the

H_2 released from the HSS caters to the H_2 demand. The other part generates electricity using the FC (fig. 4.4b). The HSS provides arbitrage benefit since H_2 is produced by the P2H unit and stored in the HSS when the grid power price is low and there is abundant RES generation. As the grid power price increases, the stored H_2 is converted back to electricity using FC. The FC and the BESS provide islanding reserves during this period (see fig. 4.6).

fig. 4.11 and fig. 4.12, respectively, show the line loading and bus voltage profiles for scenarios S#1 and S#2. The maximum line loading in scenario S#1 is $\sim 95.35\%$ (line 3 during hour #17). In scenario S#2, the peak line loading is $\sim 77.80\%$ (line #3 during hour #18) in a day. In scenario S#1, the minimum bus voltage in a day is 0.9989 p.u. (bus #5 during hour #2). On the other hand, the maximum bus voltage in a day for scenario S#1 is 1.0015 p.u. (bus #3 during hour #18). The minimum bus voltage in a day is 0.9989 p.u. (bus #4 during hour #2), while the maximum bus voltage in a day is 1.0013 p.u. (bus #3 during hour #18) for scenario S#2. Therefore, the proposed EMS with islanding constraints enforces line rating and bus voltage constraints. Earlier research on electricity-H_2 sectoral coupling primarily emphasised the operational and economic advantages [12, 78, 79, 80, 81, 86]. However, a significant gap exists in these studies, as they overlooked the DCμG network model and associated operating constraints within the DCμG. This oversight could result in unaddressed network constraint violations, which are crucial for ensuring the secure operation of the DCμG. By contrast, the EMS proposed in this chapter ensures that DCμG network operating constraints are not violated. The GT remains off throughout the day. Otherwise, the carbon emission due to GT generation increases the carbon trading costs.

fig. 4.13 shows the temperature of the electrolyzer stack. We observe that the electrolyzer stack temperature lies within allowable limits (between 60° C and 80° C) in both scenarios. Therefore, apart from power rating constraints, the proposed EMS also successfully enforces equipment level constraints like electrolyzer stack temperature. In other words, the proposed EMS meets the operating constraints of the equipment deployed in the electricity–H_2 DCμG. The indoor temperature of a room cooled by the TCL should lie between $75.20°F$ and $80.60°F$ for the comfort of the occupants. From fig. 4.9, we observe that the indoor temperature of a room remains within the range throughout the day even when the TCL participates in the DR program. Therefore, the DR program

Table 4.5: Impact of flexibilities

HSS	BESS	DR	DCμGO profit ($/day)	Electricity cost of flexible consumers ($/day)	RES curtailment (%)
✓	✓	✓	**138.55**	**17.30**	**0.00**
×	✓	✓	2.45	16.10	36.01
✓	×	✓	137.39	17.12	0.00
✓	✓	×	135.54	21.11	0.00

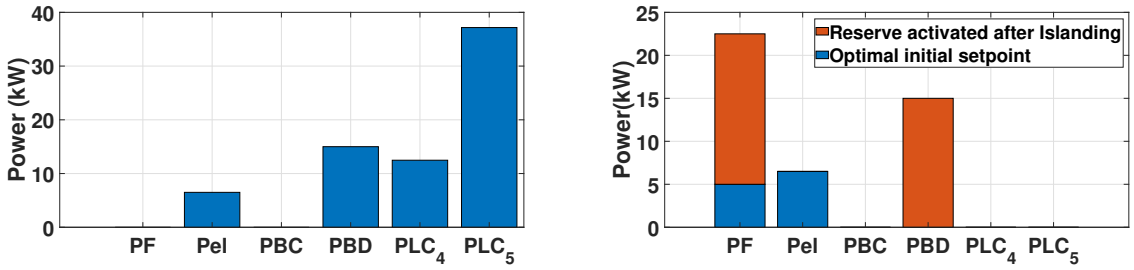

(a) Scenario S#1

(b) Scenario S#2

Figure 4.14: DER powers after islanding at hour #6-Mode 2

considered in the proposed bi-level SG-based EMS also meets the consumer requirement and consumer's apparatus-level operating constraints.

4.3.2.4 Impact of various flexibilities in S#2 with mode 2 optimisation

The impacts of various flexibilities are shown in table 4.5. The profit of the DCμGO reduces drastically ($\sim$ 98.23%) when the HSS is not considered. The FC remains off while the GT remains on for the entire day. Also, there is $\sim$ 36.01% curtailment of WPG power in the absence of the HSS. The above results illustrate the benefits of electricity-H_2 sectoral coupling in a DCμG framework, which is one of the focus areas of this work. HSS has high energy density and provides a long-duration large-scale energy storage option in the form of H_2 during periods of low electricity price in the wholesale market and high RES generation. The H_2 stored in the HSS is converted to electricity to meet the electricity demand when the electricity price in the wholesale market is high and RES generation is low, thereby providing arbitrage benefit (discussed in details in section 4.3.2.3). The arbitrage benefit cannot be availed without the HSS, and excess RES generation is

curtailed since the BESS alone cannot store the excess RES generation. Therefore, the operating profit of the DCμGO reduces, and RES generation has to be curtailed in the absence of the HSS, as seen in the results. The absence of the BESS reduces the DCμGO profit by $\sim 0.84\%$ since the arbitrage benefit provided by the BESS cannot be availed in this case. The role of the BESS in yielding arbitrage benefit has been explained in detail in section 4.3.2.3. If the DR program is not activated, the DCμGO profit reduces by $\sim 2.17\%$, and the electricity usage cost of flexible consumers increases by $\sim 22.02\%$. The above results underscore the importance of coordinating the DR implementation scheme with the scheduling strategy of the DCμGO, which is an objective of the EMS design. The DCμGO sets low RPP for the electricity consumers during off-peak periods when the electricity price in the wholesale market is low (discussed in detail in section 4.3.2.3), resulting in a shift of flexible electrical demands to off-peak periods when DR is implemented. Therefore, the DCμGO procures electricity at a low cost from the upstream grid for catering to the electricity demands. Hence, the operating cost of the DCμGO reduces, and the profit increases. On the other hand, flexible consumers also benefit due to the low RPP. Therefore, the profit of the DCμGO reduces, and the cost of electricity use by the consumers increases when the DR program is not implemented.

4.3.2.5 Analysis of an unintended islanding event

Let us assume that unintended islanding occurs at hour #6. The powers of the DERs just after islanding are shown in fig. 4.14. In scenario S#1, the FC and GT are OFF before islanding. Hence, they cannot provide islanding reserves immediately after unintended islanding (see fig. 4.14a). The BESS discharges 15 kW (see fig. 4.14a). Since the DCμG imports 50 kW of power from the upstream grid before islanding, the loss of the grid cannot be fully compensated, necessitating load-shedding (12.48 kW and 37.17 kW at buses #4 and #5, respectively) immediately after islanding (see fig. 4.14a). The minimum bus voltage is 0.95 p.u. at bus #5, and the maximum bus voltage is 0.9506 p.u. at bus #3. Line #5 is most heavily loaded ($\sim 30.9\%$). In scenario S#2, the DCμG imports 32.50 kW from the upstream grid before islanding. Also, the FC is ON. After the unintended islanding, the FC increases its generation from 5 kW to 22.50 kW (i.e., an increase of 17.50 kW, see fig. 4.14b), and the BESS discharges 15 kW to compensate for the loss of the grid. According to the optimal set point obtained from the EMS for

grid-connected operation, the BESS was in floating mode (i.e., neither charging nor discharging) before the islanding event. After islanding, the BESS activates its islanding reserve and starts discharging 15 kW to compensate for the loss of the main grid (see fig. 4.14b). Therefore, no load-shedding is required. The minimum and maximum bus voltages are 0.95 p.u. at bus #5 and 0.9513 p.u. at bus #3, respectively. The maximum line loading is $\sim$ 46.5% (line #6). Therefore, incorporating islanding constraints in the EMS avoids load-shedding immediately after an unintended islanding event. Therefore, the simulation study validates that the designed EMS meets the objective of minimising load curtailment after unintended islanding. Further, line loading, bus voltage, and equipment operating security constraints are also met after the unintended islanding, guaranteeing secure operation, as considered an objective during the EMS design stage. Note that secure operation without violation of network and equipment operating security constraints and minimum load curtailment cannot be guaranteed by the EMSs reported in most previous studies since the islanding capability of the DCμG was not incorporated in the above studies [23, 27, 29, 31, 34, 41, 66, 104]. The EMS proposed in this chapter addresses this limitation of previous studies.

4.4 Conclusions

A bi-level SG-based probabilistic EMS is proposed for a grid-connected electricity-H_2 DCμG. The grid-connected DCμG is equipped with WPG, SPG, GT, P2H, H2P, BESS, and HSS units. All the above resources are controlled by the DCμGO. Moreover, the DCμGO caters to consumers with non-flexible and flexible (TCL and PHEV) electricity demands. The difference between the proposed EMS scheme and previously reported ones is the consideration of electricity-H_2 sectoral coupling and HESS in a DCμG framework, incorporation of islanding constraints to hedge the risk of uncertain islanding events, and DR implementation taking into account the DCμG network level, DCμG equipment level, and consumer's apparatus level operating security constraints. Further, the EMS is designed considering correlated and uncorrelated input uncertainties. Correlation between input RVs is modelled using the Copula theory, embedded in a Monte-Carlo dynamic averaging framework, and included in the EMS to reduce the risk of dispatch strategy owing to input uncertainties. The scheduling strategy aims to balance the interests of

the DCμGO and the consumers participating in the DR program. It is accomplished by designing the EMS by a leader-follower bi-level SG game, in which the DCμGO is the leader and consumers are followers. The DCμGO optimally schedules all resources under its control and sets the dynamic RPP to maximise its profit. The consumers respond to the RPP set by the DCμGO by adjusting the flexible electricity demand to minimise the cost of electricity consumption. The new electricity demand pattern is conveyed to the DCμGO. The DCμGO responds by re-optimising its resources, setting a new RPP, and conveying the same to the consumers. The iterative process continues till a SG equilibrium is established. The bi-level problem is solved as a single-level MILP problem by successively using the KKT conditions of the lower-level problem, the big-M method, and the concept of strong duality. The main conclusions from the simulation studies are as follows:

1. The proposed EMS model successfully achieves SG equilibrium, balancing the interests of the DCμGO and flexible consumers. Therefore, simulation results validate the objective of contribution#3 and address gap #3 of previous work threads.

2. Incorporation of islanding constraints increases the operating cost and reduces the profit of the DCμGO since less economical units also remain on to provide islanding reserves. For the studied test system, the DCμGO profit reduces by $\sim$ 21.3%, and the operating cost of the DCμGO increases by $\sim$ 2.26% when the islanding constraints are incorporated into the scheduling strategy. However, the operation of the DCμG becomes secure in the event of unintentional islanding. For instance, an unintentional islanding event at hour #6 leads to load curtailment of 12.48 kW and 37.17 kW at bus #4 and bus #5, respectively, when the islanding constraints are not considered in the scheduling strategy. On the other hand, load-shedding is not required if islanding constraints are embedded in the EMS. Therefore, simulation results meet the objective of contribution#2 and address gap#2 of the previously reported literature. The electricity usage cost of the consumers is not sensitive to islanding constraints.

3. Proper coordination of HSS, BESS, TCL, and PHEVs enhances the profit of the DCμGO. The HSS significantly affects the operating economy. The profit of the DCμGO reduces by $\sim$ 98.23% when the flexibility of the HSS is not leveraged in the

scheduling algorithm. On the other hand, the absence of BESS flexibility reduces the DCμGO profit by $\sim$ 0.84%. HSS also mitigates curtailment of RES generation. The RES generation curtailment is $\sim$ 36.01% if the HSS is not present in the DCμG. The simulation results underscore the advantages of electricity-H_2 sectoral coupling and coordinating DR implementation with the optimal scheduling of electricity-H_2DCμG. In other words, the results justify objectives of contribution#1 and contribution#3 and highlight the improvements over previously reported work (gap#1 and gap#2).

4. Proper DR implementation also reduces the cost of electricity usage of flexible consumers and enhances the profit of the DCμGO. The DCμGO profit reduces by $\sim$ 21.7%, and the electricity usage cost of flexible consumers increases by $\sim$ 22.02% if the DR program is not implemented. The simulation study highlights the benefits of DR integration with the electricity-H_2DCμG scheduling problem, condoning the importance of contribution#3 and the gap area of previous studies (gap#3).